Tunneling RFID Tags for Long-Range and Low-Power Microwave Applications

Francesco Amato, *Member, IEEE*, Christopher W. Peterson, *Student Member, IEEE*, Brian P. Degnan, *Member, IEEE*, and Gregory D. Durgin, *Senior Member, IEEE*

***Abstract*—Backscatter modulation in radio frequency identification (RFID) tags will potentially connect billions of tomorrow's devices to the Internet-of-Things. Current passive RFID systems have power constraints that limit RFID tag communication to short ranges, but these limitations can be overcome by employing reflection amplifiers. In this paper, we show that negative differential resistance devices, such as tunnel diodes, exhibit 27 dB more gain and 10 dB lower power consumption than state-of-the-art reflection amplifiers. Two 5.8 GHz prototypes using off-the-shelf tunnel diodes show reflection gains of 40 dB and 29 dB for a total biasing power consumption of 45 μW and 39 μW, respectively, at impinging RF power levels as low as −84 dBm. A 5.8 GHz RFID link of 23 m was achieved when transmitting only −14 dBm of effective isotropic radiated power from a transceiver with a sensitivity of −90 dBm.**

***Index Terms*—RFID, long-range backscattering, backscattering, backscatter modulation, IoT, Internet of Things, CMOS integrated circuits, tunnel diode, quantum MOS, negative differential resistance, tunneling reflector, radio propagation.**

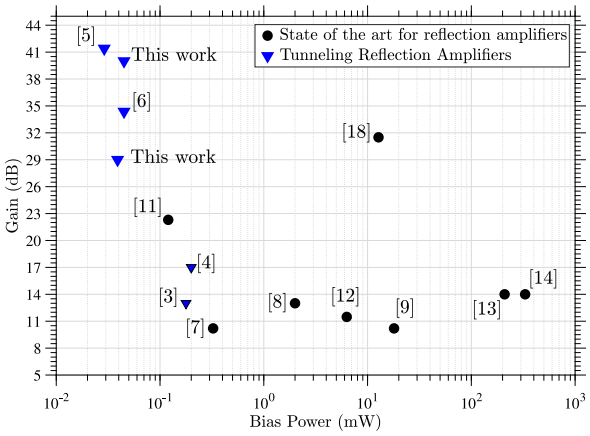

Fig. 1. State-of-the-art of reflection amplifiers. Comparisons of return gains and required biasing DC powers. An earlier version of this plot is published in [6].

I. Introduction

THE EMERGING applications in wearable sensors, localization, machine-to-machine communications, and Internet-of-Things (IoT) devices require long-range wireless connections, small form factors, high-bandwidth, and, perhaps most importantly, *low power consumption*. One way to drastically reduce the current power bottleneck for wireless nodes is to employ a tunneling tag in backscatter radio links. This paper demonstrates how to build a 5.8 GHz Tunneling Reflector for a Tunneling Tag [1], [2] capable of exchanging information at kilometer-scale ranges while consuming less than 45 μW of power. The use of a tunneling reflector at the terminals of a microwave antenna allows an RF node to remove the two most power consumption elements of a radio – its transmit power amplifier and RF synthesizing circuitry.

Our proposed approach retrieves information from an RFID-style transponder, or tag, consisting of an antenna and a programmable switching load. The tag is remotely activated by a continuous wave (CW) carrier sent by a reader and reflects back modulated data. The tunneling tag is achieved using a reflection amplifier with a locally DC-biased tunnel diode at the terminals of the antenna. Fig. 1 and Table I summarize our results and those reported in the research literature on gains and power consumption of reflection amplifiers [3]–[18]. Gains as high as 31.5 dB were reported for biasing powers falling in the range between 0.12 mW and 330 mW. These results employ pHEMT, FET and bipolar transistor components; a Josephson junction exploiting the tunneling effect using superconductors at cryogenic temperatures has shown a high sensitivity (31.5 dB gain) and low power consumption [10] while recent work with tunnel diodes have achieved gains as high as 40 dB for biasing powers lower than 45 μW [5], [6].

In this paper, we present the prototype of a tunneling reflector (TR) that would act as the switching load for the tunneling tag; it contains details about the tunnel diode model, a description of the amplifier topology and a new set of wired and wireless experiments. While its previous versions were tuned at 5.45 and 5.55 GHz [6], this newly designed model works in the 5.8 GHz ISM band (5.725 - 5.875 GHz). Section II

Manuscript received January 4, 2018; revised June 7, 2018; accepted June 29, 2018. Date of publication July 4, 2018; date of current version September 4, 2018. This work was supported by National Science Foundation under Grant 1408464. *(Corresponding author: Francesco Amato.)*

F. Amato was with the School of Electrical and Computer Engineering, Georgia Institute of Technology, Atlanta, GA 30332 USA. He is now with the Institute of Communication, Information and Perception Technologies, Sant'Anna School of Advanced Studies, 56127 Pisa, Italy (e-mail: f.amato@gatech.edu).

C. W. Peterson is with the Department of Electrical and Computer Engineering, University of Illinois at Urbana–Champaign, Urbana, IL 61801 USA (e-mail: cwpeter2@illinois.edu).

B. P. Degnan and G. D. Durgin are with the Department of Electrical and Computer Engineering, Georgia Institute of Technology, Atlanta, GA 30332 USA (e-mail: degs@gatech.edu; durgin@gatech.edu).

Digital Object Identifier 10.1109/JRFID.2018.2852498

TABLE I
OVERVIEW OF REFLECTION AMPLIFIERS AVAILABLE IN LITERATURE

Reference	Year	Device Type	Part number	Substrate	DC Bias Power (mW)	Gain (dB)	P_{out}/P_{DC} %	Bias Volt. (V)	Bias Curr. (mA)	RF Input (dBm)	Freq. (GHz)
This work	2017	tunnel diode	MBD5057-E28	Ge	0.045	40	0.7	0.09	0.5	-75	5.8
					0.039	29	0.008	0.11	0.354	-84	
[3]			AI301A	GaAs	0.178	13	11.2	-	-	-30	0.915
[4]					0.2	17	25	0.2	1		0.890
[5]	2015		MBD5057-E28	Ge	0.029	41.4	0.03	0.069	0.418	-92	5.8
[6]					0.045	34.4	0.61	0.08	0.566	-70	5.45
[7]	2014	bipolar trans.	BFT25A	Si	0.325	10.2	0.031	0.755	0.431	-50	0.920
[8]	2013		BFP405		2	13	0.003	2.5	0.8	-55	5.25
[9]		MESFET	CFY30	GaAs	18	10.2	5.7e−4	3	6	-	4.5
[10]		Josephson junc.	-	-	-	30	-	-	0.054	-145	2.7
[11]	2012	MOSFET			0.120	22.3	0.009	0.8	-	-71.9	4
[12]	2011	pHEMT	NE32584C	GaAs	6.3	11.5	1.8e−3	0.7	9	-	5.8
[13]	2008		-		209.3	14	0	2.3	91	-75	21.2
[14]	2006		CGY2134UH		330		0.0002	2.2		-45	
[15]	2003		NE32584C		-	8.1	-	-	-		6.26
[16]	1991	MESFET	NE71083			12				-	9
[17]	1979	FET	-		2000	16	8e−6	4	500		13
[18]	1972	avalanche diode		-	12.75	31.5	350.3	85	0.150	-15	7.4

describes the basic operations of a reflection amplifier, provides a state-of-the-art of this technology in the research literature and gives an overview on natural negative differential resistance in tunnel diodes. The design and fabrication of a tunneling reflector is provided in Section III. In Section IV, a new set of experimental data describe the electromagnetic characteristics of two manufactured prototypes and, following the experiments outlined in [5], wireless measurements using a tunneling tag are compared with a semi-passive tag. Finally, Section V highlights the achievable ranges of a tunneling tag and compares them with both ideal passive and semi passive tags at 5.8 GHz.

II. BACKGROUND

Backscatter communication is usually implemented with *load modulation* of one or more antennas. Load modulation results in a form of amplitude and phase-shift keying that can then be detected by a reader [19]. The most common form of load modulation operated by an RFID tag is binary load switching, where the impedance of an antenna is switched between two passive loads (e.g., open and short) to enable modulation of the backscattered signal. In these communication systems, the power link budget is defined by the following expression:

$$P_R = P_T G_T G_R G_t^2 \left(\frac{\lambda}{4\pi r}\right)^4 M; \tag{1}$$

with P_T the power transmitted by the reader; G_T and G_R the gains of the transmitting and receiving antenna, respectively; G_t the gain of the tag antenna; λ the wavelength of the carrier; r the reader-to-tag distance; P_R the power level detected at the reader and M the tag modulation factor [20]. Passive loads, typically used in both passive and semi-passive tags, result in a modulation factor M lower than 1. Reflection amplifiers replace at least one of the passive loads with an active impedance Z_L that improves the modulation factor M by adding amplification capabilities to the RFID tag.

A. Basic Operation of a Reflection Amplifier

Reflection amplifiers are characterized by a negative load impedance Z_L that, at the cost of a certain amount of biasing voltage V_{bias}, can amplify and backscatter an impinging RF signal P_{in} at frequency f_{in}:

$$Z_L(f_{in}, V_{bias}, P_{in}) = -R_L + jX_L, \quad R_L > 0. \tag{2}$$

The load of a reflection amplifier may also vary as a function of secondary parameters, such as device temperature. When a reflection amplifier is properly matched to an impedance $Z_A(f_{in}) = R_A(f_{in}) + jX_A(f_{in})$, such that:

$$X_A(f_{in}) + X_L(f_{in}, V_{bias}, P_{in}) = 0, \tag{3}$$

then, the DC power provided by the biasing source converts into RF power that is added, upon reflection, to the impinging signal. The principle of conservation of energy is preserved and the added gain corresponds to the negative and greater than 1 reflection coefficient Γ of the reflection amplifier:

$$|\Gamma|^2 = \left|\frac{Z_L - Z_A}{Z_A + Z_L}\right|^2 = \left|\frac{R_A + R_L}{R_A - R_L}\right|^2 > 1. \tag{4}$$

Clearly, by properly choosing R_A, positive gains can be obtained. In principle, Eq. (4) is limited by the finite size of the negative-resistance region of practical, active electronics. Eq. (4) is also practically limited by the need to suppress spontaneous oscillatory modes in the device.

Of course, by adding power to the reflected signal, the reflection amplifier is converting DC bias power into RF power through a form of *injection locking* [21]. The locking RF range $2\Delta f$ for such a device is given by [22]:

$$\frac{2\Delta f}{f_{in}} = \frac{2}{Q}\sqrt{\frac{P_{in}}{P_0}} \tag{5}$$

which depends on the quality factor Q of the circuit, the injected power P_{in}, the locked power P_0 and the center frequency f_{in}; with Δf being the one-side locking bandwidth.

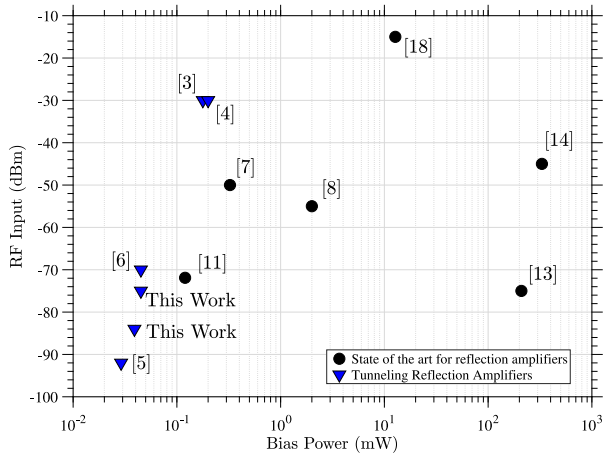

Fig. 2. State-of-art of reflection amplifiers. Comparing the RF input powers with the required DC biases as reported in Table I.

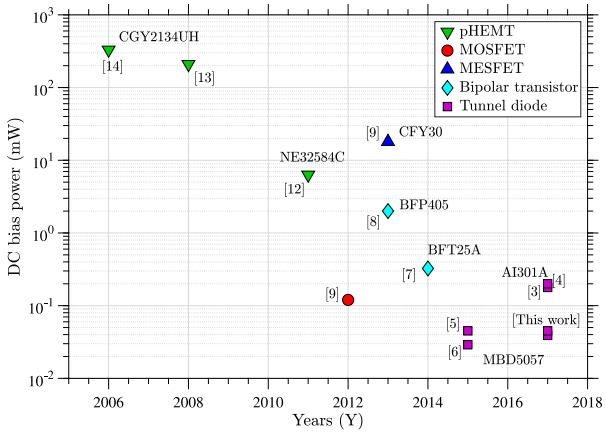

Fig. 3. Data from Table I show a decreasing power consumption of reflection amplifiers in recent years; tunnel diode-based reflectors lead the trend.

If G is the gain of the reflection amplifier, we can rewrite Eq. (5) as

$$\Delta f = \frac{f_{in}}{Q\sqrt{G}} \tag{6}$$

Thus, a reflection amplifier can lock onto a broader range of input frequencies Δf if the circuit Q-factor and/or the amplifier gain is reduced.

B. State-of-the-Art Reflection Amplifiers

Tuning and modulation capabilities of reflection amplifiers based on pHEMT, FET and bipolar transistor devices have already been explored in [7]–[9] and [11]–[17]. These devices, of course, provide an extraordinarily low-cost and flexible technology for building RF reflection amplifiers, but do not achieve the lowest power consumption.

The idea of using a reflection amplifier to improve backscattering of an incident RF signal is reported in [23] while Cantu and Fusco [14] highlight the difficulties of amplifying a signal at the desired frequency: parasitic components can produce a 2-3 GHz shift from the center frequency at K band (18–27 GHz) and an additional phase shift (750 MHz) is observed when the biasing voltage level varies. As shown in [13], turning on and off the biasing voltage can be used for amplitude and phase modulation of the backscattered signal and a full-duplex communication to improve both the return and the forward links is presented in [8]: the authors incorporated a *transmission* amplification capability to amplify the received forward link signal before modulating, reflecting and amplifying it for the return link data stream.

Several researchers have built upon these early results suggesting different types of reflection amplifiers [7]–[9], [11]–[17]. Table I gives an overview of the results reported in the research literature and shows, through the gain-per-bias-power ratio, how much gain (in dB) is added to the reflected RF signal per units of μW. A figure of merit comparing the maximum achieved output powers with the corresponding required bias have also been computed, where possible. Fig. 1 focuses the attention on both the achieved gains (up to 31.5 dB) and the power requirements (ranging between 0.12 mW and 330 mW). The maximum achievable ranges and the battery lifetime can be inferred by looking at the data points in Fig. 2. As shown, a tunnel diode-based reflection amplifier can achieve RF output powers up to -35 dBm with biasing powers below 0.1 mW. Reflectors mounting avalanche diodes can achieve even higher RF outputs at the cost of more biasing power [18]. As shown in Fig. 3, the power consumption of reflection amplifiers has been decreasing during the recent years and tunnel diode-based reflection amplifiers can be a natural step towards less power-hungry electronics. The use of negative differential resistance devices to fabricate reflection amplifiers is possible [24] and the achieved high gains (up to 40 dB) and the low biasing power requirements (45 μW) in [5] and [6] suggested the fabrication of a tunneling RFID tag capable of amplifying and modulate the backscattered signal by applying a proper modulating bias voltage (Fig. 4) to reach hundreds meters of range [1], [2].

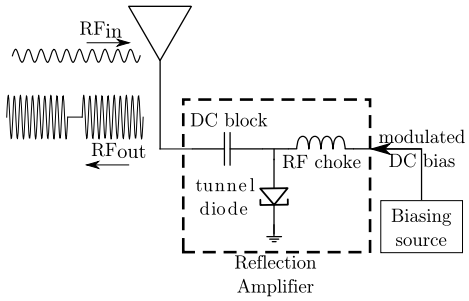

Fig. 4. Block diagram of a tunneling RFID tag.

C. Quantum Tunneling Effect in Tunnel Diodes

Research literature has extensively studied some interesting two-port devices having the common property of displaying a natural negative differential resistance when properly biased. Among them, the IMPATT (IMPact Ionization Avalanche Transit Time) diodes [25], the Gunn diodes [26]–[28] and the Esaki diodes are the most common.

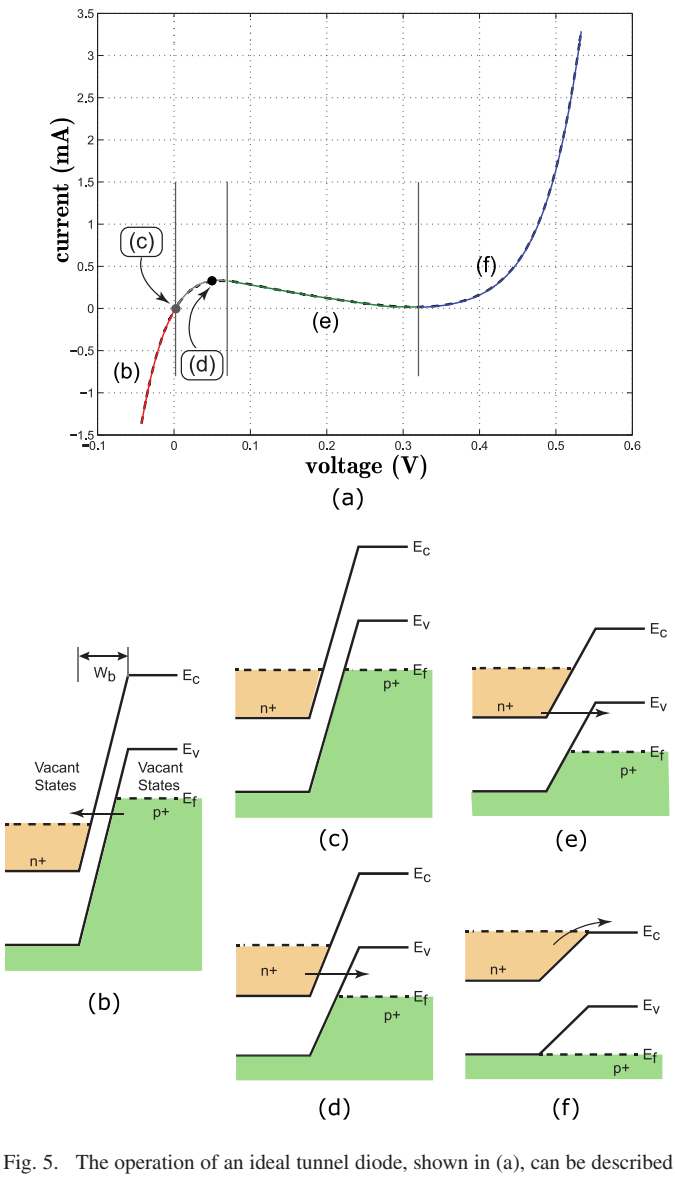

Fig. 5. The operation of an ideal tunnel diode, shown in (a), can be described through several band diagrams. The highly doped device increases the probability of tunneling. The overlap of states allows the electrons to tunnel through the barrier; the higher is the overlap, the higher is the tunneling current across the barrier as shown in (b) and (d). At higher bias (e), the overlap of states decreases and so does the tunneling current. In (f), the current is dominated by injection of carriers over the barrier in the classical diode behavior.

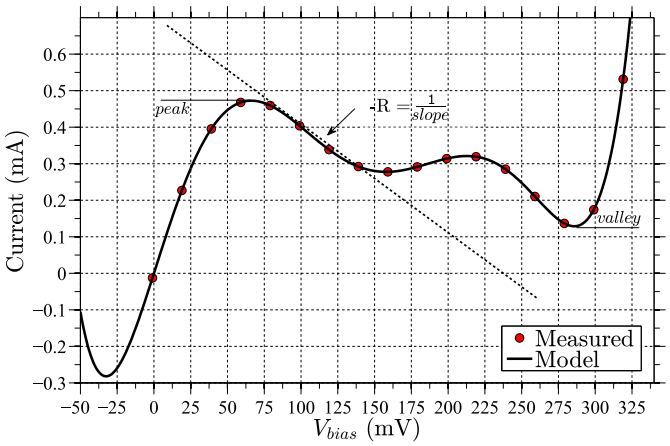

Fig. 6. Measured I-V characteristic of the tunnel diode MBD5057-E28 at 300 K and the model used for simulations.

A tunnel diode (also known as Esaki diode) is the first manufactured semiconductor where quantum tunneling was observed. After its discovery [29], [30], its physics was extensively discussed [31]. A tunnel diode consists of a p-n semiconductor junction with a high concentration of donors and acceptors (p^+n^+). This construction results in empty states in proximity to electrons separated by a barrier; tunneling takes place because of overlap of the energy states, that is, states filled with electrons in conduction band and states filled with holes in valence band are aligned across the tunneling barrier. Electrons increase their probability of tunneling through the barrier when proper external biasing voltage is applied [22].

In Fig. 5, the I-V curve of a tunnel diode is marked with corresponding band conditions. For a device under a reverse bias (Fig. 5b), the number of electrons that are able to tunnel increases, tunneling takes place and a reverse current is observed. At zero bias, (Fig. 5c), no electrons are across from empty states to which they can tunnel and no current is displayed. For a small forward bias (Fig. 5d), electrons at the bottom of the conduction band are available to tunnel to the empty states at the top of the valence band, and the forward current increases with an increased bias until a peak is reached: the peak occurs when the overlap between the filled states on the conduction band and the empty states on the valence band is maximized. However, as the bias increases, the overlap is reduced below the maximum possible and the negative differential resistance region manifests; tunneling fades and the current decreases (Fig. 5e). The ever increasing bias moves the device out of the tunneling behavior to the characteristic $p-n$ junction behavior as shown in Fig. 5f.

The tunneling effect summarized above allows the construction of tunnelling-based devices that can be used for different applications [32]: besides behaving like a Schottky diode when large forward biases are applied, a heterostructure backward tunnel diode can be used for energy harvesting applications [33]. Finally, the decreasing current as effect of the increasing bias gives to the tunnel diode a natural negative differential resistance $-R$ that can be used to design a reflection amplifier.

III. Tunneling Reflectors

The low biasing requirements and the natural negative differential resistance of a tunnel diode make this device a good candidate to realize a Tunneling Reflector (TR) with high reflective gain and low power consumption. A prototype was fabricated and tested in laboratory using the off-the-shelf tunnel diodes MBD5057-E28 [34].

A. Device Characterization

Tunnel diode #0 was used to characterize the device and develop a design model. The I-V characteristic (Fig. 6) was measured at room temperature (300 K) using a DC power supply to bias the device, mounted on a PCB, and an HP

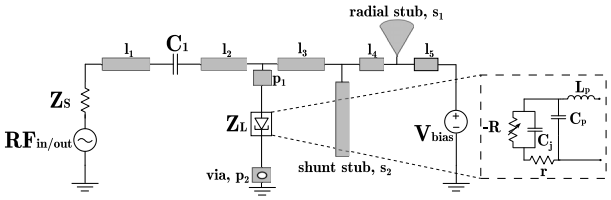

Fig. 7. Circuit schematic of a tunneling reflector with a shunt stub, s_2, at distance $l_3 = 40$ mil from the diode; the equivalent circuit of the tunnel diode is highlighted: $C_j = 0.03$ pF is the internal junction capacitance, $C_p = 0.8$ pF and $L_p = 0.4$ nH are the packaging parasitics and $r = 0\ \Omega$ is the negligible linear resistance; a voltage controlled source models the nonlinear junction resistance through Eq. (7).

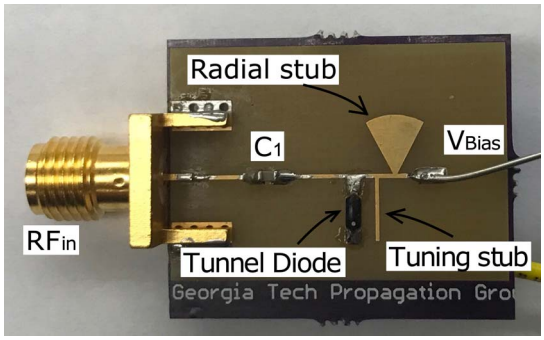

Fig. 8. Microstrip line structure of the fabricated Tunneling Reflector as in [5]: the shunt stub is 180 mils (4.9 mm) long and 14 mils (0.3 mm) wide. Its exposed trace, not covered with silkscreen, can be used for tuning purposes, if necessary. A capacitor C_1 of 1.5 pF was used as DC block. Two identical boards were manufactured to test two MBD5057-E28 tunnel diodes (#1 and #2).

34401A precision digital multimeter to measure the current. The voltage range spanning from 70 mV to 280 mV has a non-uniform slope due to tunneling through higher-level confined states in the tunnel diode [29]; this results in two separated intervals with negative differential resistances: from 70 mV to 160 mV ($|-R| = 465\ \Omega$) and from 210 mV to 280 mV ($|-R| = 426\ \Omega$). In the region between 160 mV and 210 mV, there is little or no negative differential resistance so no significant RF amplification of an impinging signal is expected. For this particular device model, the reduced span of uniform negative differential resistance region limits amplification to only low power RF signals. Although low power levels are typically encountered in RFID communications, a more uniform characteristic curve can extend the results obtained in this work to higher input power levels. The device operates up to 18 GHz, have a peak-to-valley current ratio of 3, and is fabricated using rapid thermal diffusion on Germanium substrate.

B. Circuit Design

To use a tunnel diode as reflection amplifier, the following criteria need to be met [24]: bias the tunnel diode in the negative differential resistance region of its characteristic curve; present the transmission line with a suitable negative resistance at the center frequency f_{in}; reduce Γ to acceptable limits at frequencies away from f_{in}; and maintain stability. Keysight Advanced Design System (ADS) and the Harmonic Balance method were used to simulate and design a microstrip line version of the reflection amplifier matched at 50 Ω for low impinging power levels. After running the momentum simulation of the microstrip line, a momentum model was created and imported into a new schematic where it was connected to the lumped circuit components (DC-block capacitor, tunnel diode model, biasing power supply and RF input signal). A circulator, together with voltage and current probes, were inserted into the simulation to measure the RF input and output powers and calculate the return gains.

The circuit schematic, together with the tunnel diode MBD5057-E28 equivalent circuit, are shown in Fig. 7: an external power supply biases the tunnel diode at the desired voltage V_{bias} to amplify the RF signal input injected through a source with impedance Z_S; a radial stub s_1 isolates the biasing network from the input RF section while a capacitor, C_1, is used as DC block, finally, a shunt stub, at distance $l_3 = 40$ mil from the tunnel diode, compensates the undesired internal capacitance of the device. The small signal equivalent circuit of the diode is also highlighted: $L_p = 0.4$ nH and $C_p = 0.8$ pF account for the packaging parasitics; $C_j = 0.03$ pF represents the internal junction capacitance that, although it varies with the applied biases, it is here considered constant to simplify the design procedure. The nonlinear junction resistance is modelled through a voltage controlled source defined by:

$$I(V_{bias}) = 0.0126V_{bias} + 0.0068V_{bias}^2 - 2.6201V_{bias}^3 + 24.3383V_{bias}^4 - 84.2936V_{bias}^5 + 101.8188V_{bias}^6, \quad (7)$$

with V_{bias} being the applied biasing voltage; and the series linear resistance r is considered negligible since it is much smaller than the junction resistance. As shown in Fig. 6, the model is valid in the biasing range of interest (0 to 300 mV).

C. Board Assembly

The reflection amplifier was realized on a microstrip line [35]. The top layer with 1.4 mils of copper is separated from the ground plane by a 6.7 mils FR408 substrate [36]. The substrate has a permittivity of 3.66 and loss tangent of 0.0127 at 5 GHz. Via holes with 13 mils diameter and square pads with 15 mils side were used. The realized board (Fig. 8) uses a radial stub, s_1 to separate the biasing network from the rest of the circuit and a tuning stub, s_2. This stub allows fine tuning of the reflection amplifier at the desired center frequency f_{in} of 5.8 GHz, if necessary. Two tunnel diodes (#1 and #2) were mounted on two identical boards; Johanson Technology S603DS 0603 capacitors were used. It is important to highlight that the tunnel diodes, because of their nature, might have slightly different behaviours respect to the tunnel diode #0 used for modeling purposes. Moreover, the tunnel diodes have long leads that need to be cut to assemble the tunneling reflector. Cuts of different length, the ± 0.10 pF tolerance of the capacitors, and the structural difference of tunnel diodes #0, #1 and #2 showed a slightly different performance of the fabricated prototypes.

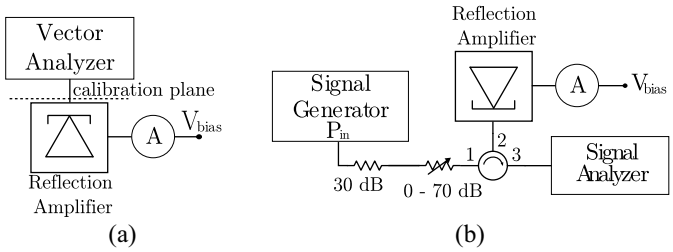

Fig. 9. Setups used to collect experimental data. a) Reflection measurements on VNA E5071B with avg. 16. b) Reflection measurements with circulator, signal generator E8247C and signal analyzer CXA-N9000A. Signal analyzer setup: resolution BW 3 kHz, video BW 100 kHz, avg. 10, span 1 MHz.

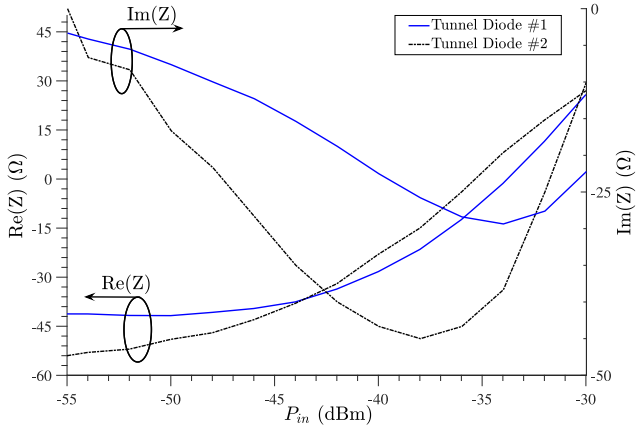

Fig. 10. Measured impedance of the two reflection amplifiers for variable RF input powers at 5.8 GHz, when optimum biases are applied.

IV. Experimental Results

A. Tunneling Reflector (TR)

Setups for measuring the reflective outputs of the TR are shown in Fig. 9. In both setups, an ammeter recorded the average DC current drawn by the TRs during measurements. In setup a), a vector network analyzer measures the S_{11} parameters of the TRs while in setup b), an RF spectrum analyzer records the reflected and amplified RF output signals generated by the device under test and verifies that the TR locks to the desired central frequency. Step attenuators were used to attenuate the RF input signal impinging on the reflection amplifier and prevent harmonics. Attenuations introduced by each additional RF component (cables and circulator) were carefully measured and removed from the collected data.

A measurement of the impedances Z_L was possible through the setup in Fig. 9a with the calibration plane located at the SMA input port of the TR. The two reflection amplifiers were biased with proper biases to display the required negative resistance and the VNA injected RF input power levels ranging from -30 dBm to -55 dBm, with the latter being the lowest possible RF power level generated by the instrument. As expected (Eq. (2)), the impedance Z_L of the reflection amplifiers depend, among other variables, on the input power level P_{in}. In Fig. 10 it is shown how, at higher input power levels, mismatch takes place; the higher the mismatch the lower the return gains.

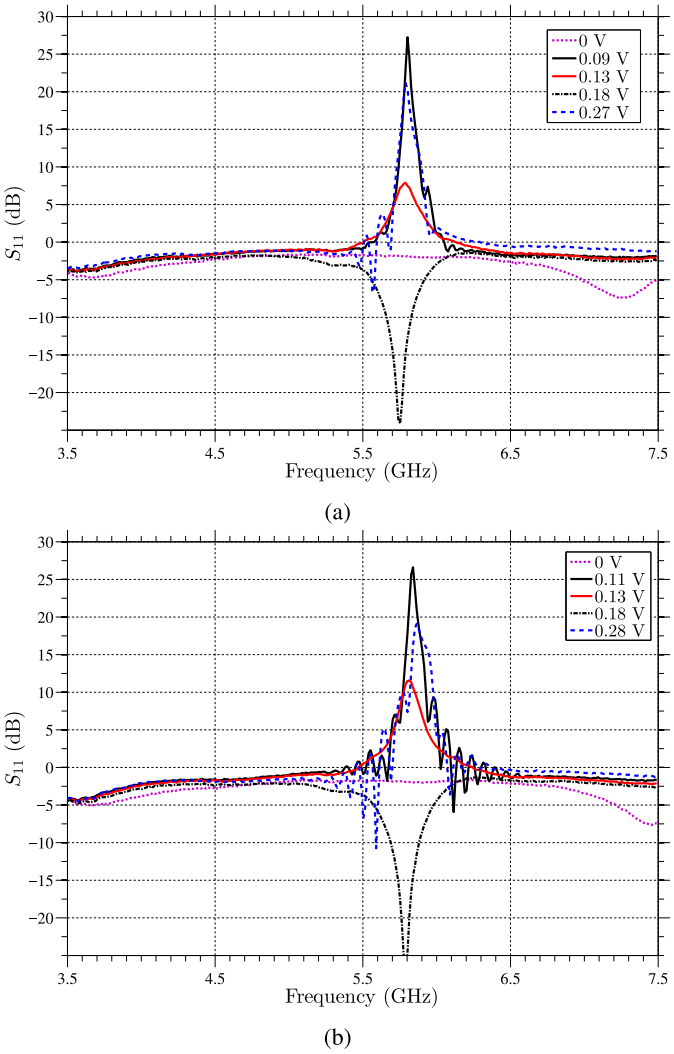

Fig. 11. S-parameter amplitudes of TRs mounting a) tunnel diode #1 and b) tunnel diode #2 at different biasing levels. RF signal input power $P_{in} = -50$ dBm, IF bandwidth 70 kHz.

Experimental results show that the designed reflection amplifiers can be used in backscatter communications for both phase and amplitude modulations by varying the biasing voltage over time. The one port S-parameter data, $|S_{11}|$, were collected using the measurement setup of Fig. 9a. The results obtained for different biasing voltages are shown in Fig. 11a and 11b for tunnel diode #1 and #2, respectively. When the biasing voltage is off, neither amplification nor emission of the TRs occur within the frequency band. When the biasing voltage forces the tunnel diode into the negative differential resistance region, the prototypes display high reflection gains for an RF input signal at about 5.8 GHz. As expected by the I-V characteristic of the tunnel diodes under test (Fig. 6), both the prototypes show a high gain for two separate biasing voltages: 90 and 270 mV for TR with tunnel diode #1 and at 110 and 280 mV for TR with tunnel diode #2; there is no amplification for biases around 180 mV.

The effect of biasing on the phase of S_{11} is shown in Fig. 12. A drastic change is evident when the biasing voltage is switched from 0 to 90 mV for tunnel diode #1 and

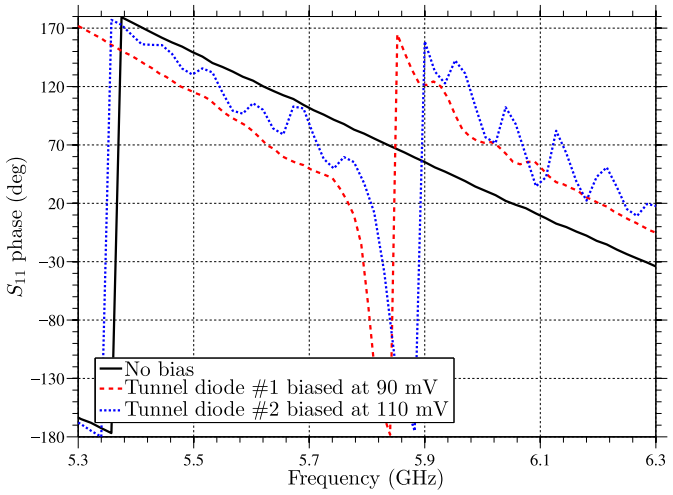

Fig. 12. S-parameter phases for the two TRs when no bias or optimal bias are applied. RF signal input power $P_{in} = -50$ dBm.

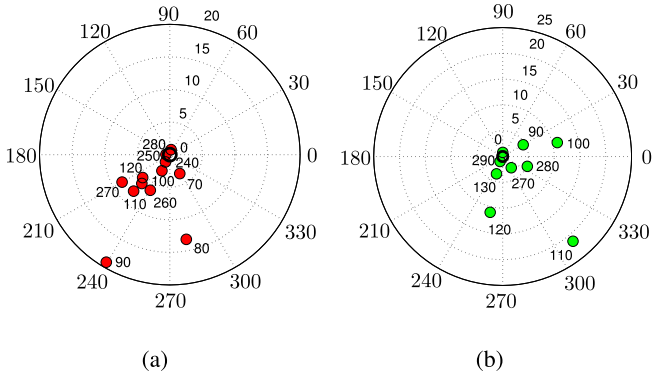

Fig. 13. Polar plots for the S_{11} parameters of the TRs for different biasing voltages (in mV); the unitary circle is highlighted in black. RF signal input power $P_{in} = -50$ dBm, RF input frequency: 5.8 GHz. Experiments done with a) tunnel diode #1 and b) tunnel diode #2.

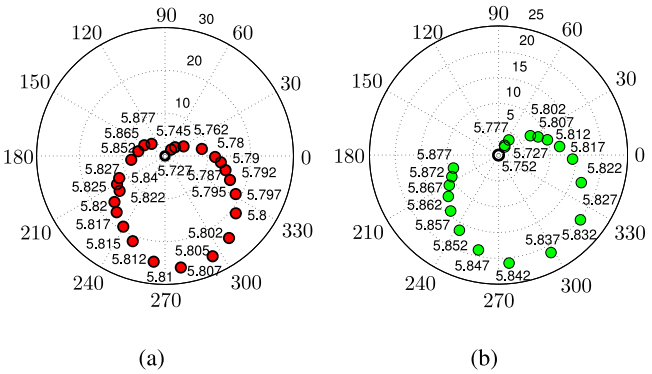

Fig. 14. Polar plots for the S_{11} parameters of the TRs for different input frequencies (in GHz) spanning in the 5.8 GHz band (5.725 GHz to 5.875 GHz); the unitary circle is highlighted in black. RF signal input power $P_{in} = -50$ dBm. Experiments done with a) tunnel diode #1 biased at 90 mV and b) tunnel diode #2 biased at 110 mV.

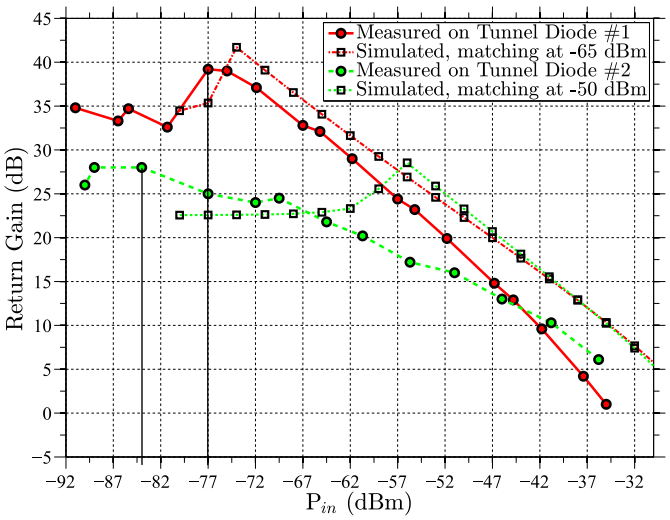

Fig. 15. TR gains, G_{TR}, as function of the RF input power at 5.8 GHz. Tunnel Diode #1: $V_{bias} = 90$ mV, $I_{bias} = 500$ μA, $P_{bias} = 45$ μW. Tunnel Diode #2: $V_{bias} = 110$ mV, $I_{bias} = 354$ μA, $P_{bias} = 39$ μW. The measured gains are compared with simulations results; the RF input powers with the highest return gains are also highlighted.

from 0 to 110 mV for tunnel diode #2 suggesting that phase modulation is possible. The TR mounting tunnel diode #1, at 5.8 GHz, has a phase of $-69°$ for $V_{bias} = 90$ mV; the TR mounting tunnel diode #2 at 5.8 GHz, has a phase of 37° for $V_{bias} = 110$ mV; finally, both the devices have a phase of 80° when no bias is applied.

Changes of both amplitude and phase of the S_{11} parameters are displayed on the Smith Chart. In Fig. 13, the effects of the biasing voltages on the reflected signals are shown: amplifications of the reflected signal occur at biasing voltages ranging in the two negative differential resistance regions of the tunnel diodes; and the optimal biasing voltages (in mV) are highlighted for the two reflection amplifiers. In Fig. 14, instead, the coverage of the 5.8 GHz band (5.725 to 5.875 GHz) is shown when the optimal bias is applied: the maximum values of S_{11} are obtained at the central frequency of 5.8 GHz and they slowly decay when the frequency approaches the band limits.

A way to test the backscattering abilities of the TRs consists in connecting the devices to a circulator to effectively separate the input from the output powers; the measurement setup shown in Fig. 9b was used to record the data reported in Fig. 15, 16 and 17.

The sensitivity of the manufactured prototypes to different levels of input power is shown in Fig. 15. The highest return gains are the following: 40 dB for RF input powers of -77 dBm on the TR with tunnel diode #1 and 29 dB for RF input powers of -84 dBm on the TR with tunnel diode #2. The two tunnel diodes were respectively biased with 90 mV and 110 mV, currents of 500 μA and 354 μA were measured for total biasing powers of 45 μW and 39 μW. At high power levels (above -35 dBm), no amplification is observed because of the mismatch between the microstrip line (50 Ω) and the impedance of the tunnel diodes (Fig. 10); at lower power levels (below -80 dBm), instead, a fall-off in gains is caused by an RF input that is too low to trigger a stronger injection locking phenomenon [21]. The experimental results agree with the simulations done in ADS. Although two identical boards were used with two MBD5057-E28 tunnel diodes, measurements

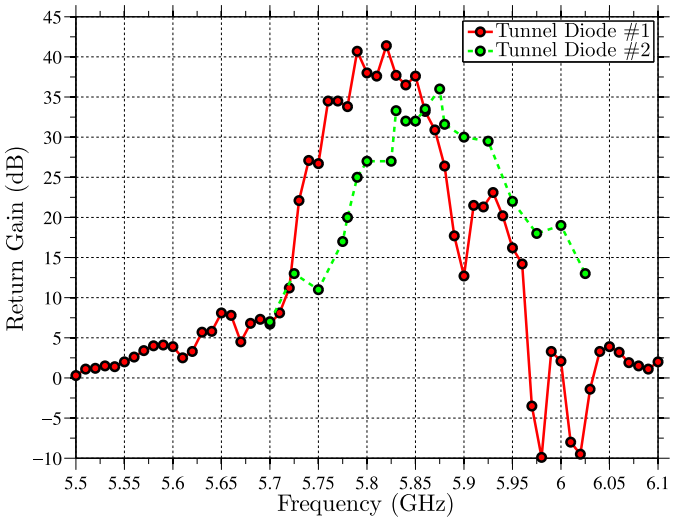

Fig. 16. TR gains, G_{TR}, as function of input frequency. Tunnel Diode #1: RF input power $P_{in} = -77$ dBm, $V_{bias} = 90$ mV. Tunnel Diode #2: RF input power $P_{in} = -84$ dBm, $V_{bias} = 110$ mV.

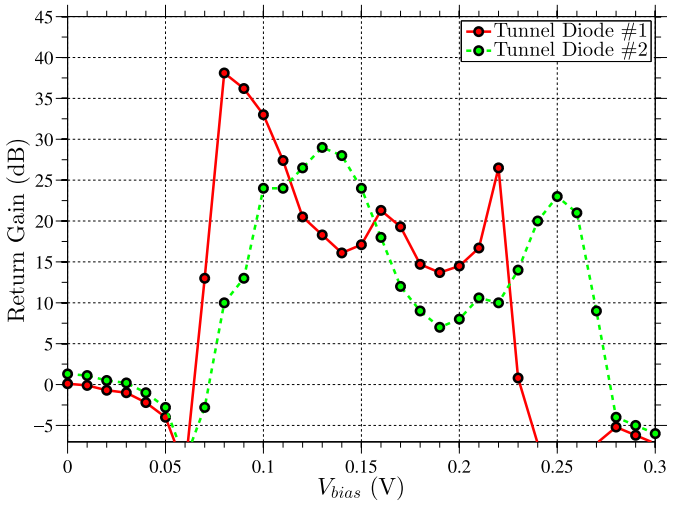

Fig. 17. TR gains, G_{TR}, as function of the V_{bias} for RF input at 5.8 GHz. Tunnel Diode #1: RF input power $P_{in} = -77$ dBm; Tunnel Diode #2: RF input power $P_{in} = -84$ dBm.

follow the simulations of devices matched at two different input power levels. This is because the two tunnel diodes do not have the same impedances and behave slightly differently from each other. There is a more pronounced deviation between measured and simulated results with Tunnel Diode #2 probably because of a mismatch created during the assembly of the PCB.

In Fig. 16, the bandwidths of the TRs are shown: at frequencies away from the 5.8 GHz band, low or no amplifications are observed suggesting that an accurate matching network would prevent the device from amplifying unwanted signals. Finally, in Fig. 17, the effects of the biasing voltage on the output gains are highlighted for both the amplifiers when a 5.8 GHz input signal is applied at optimum power levels (-77 dBm and -84 dBm respectively). As expected by the tunnel diode measured characteristic curve (Fig. 6), two peak gains are observed at two different voltage intervals.

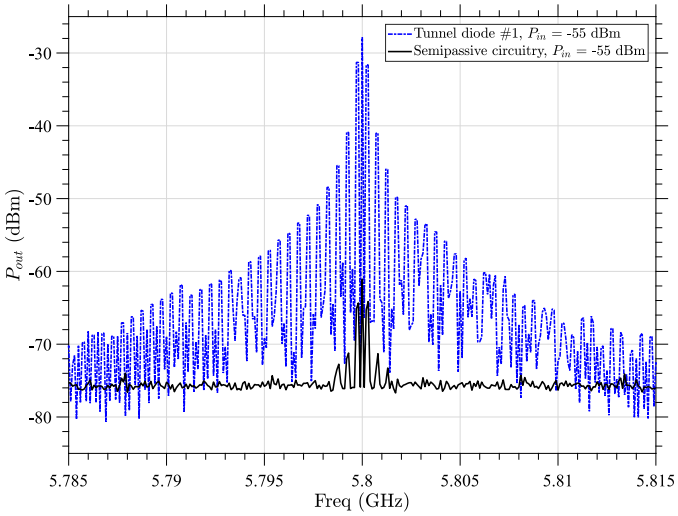

Fig. 18. Comparison of the modulating and amplifying capabilities of the TR#1 with a semi-passive tag when a low RF power input ($P_{in} = -55$ dBm) is injected. Carrier at 5.8 GHz, fundamental frequency at 250 kHz away from it, and harmonics are shown. Spectrum analyzer setup: resolution BW 20 kHz, video BW 100 kHz, sweeping time 0.12 s on 1001 points.

Differently from Fig. 11, gains are observed in the biasing range from 160 to 210 mV. The explanation can be found in the effect of the hysteresis: because many different biasing voltages were applied one after the other to trace Fig. 17, some outputs of the tunneling reflector might have been slightly influenced by the previous biasing voltages at which amplification occurs, hence the small gains in the 160 to 210 mV range.

B. Tunneling RFID Tag

Modulation with TRs can take place by biasing on and off the tunnel diode. For this purpose, a wave generator was used as the biasing source for the setup shown in Fig. 9b. The performances of TR #1 was compared with the circuitry of a 5.8 GHz semi-passive tag. A 250 kHz square wave was used as biasing source, a -55 dBm RF input was input into both the TR and the 5.8 GHz semi-passive tag circuitry. The low sensitivity of the semi-passive tag required to use -55 dBm as RF injection power although it is not the optimal RF power level at which corresponds the highest return gain on the TR. Outputs from both the TR and the semi-passive tag circuitry were measured on the signal analyzer and, through Fig. 18, their performances are compared. The benefits of using a TR over a semi-passive tag are evident; the former, not only has higher sensitivities, but it also provides substantial return gains. Additionally, a one-byte word (0xA4) was coded with Manchester encoding[1] and reproduced by the wave generator to bias tunnel diode #1 receiving an RF input power P_{in} of -55 dBm. A receiver having a high-pass cut-off frequency of 20 kHz, a low-pass cut-off of 2 MHz and a 20 dB Noise Figure, resulting in a sensitivity of -90 dBm, was used. The reflected signal was demodulated and the data were recorded

[1]The Manchester encoding used here translates each *1* as *10* and each *0* as *01* so that the word 0xA4 (1 0 1 0 0 1 0 0) translates into 10 01 10 01 01 10 01 01

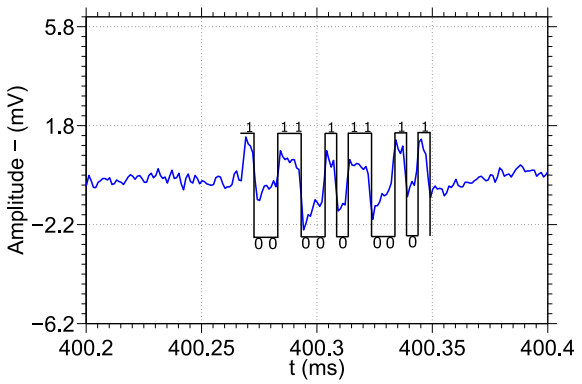

Fig. 19. Measure of the time-domain base-band signal resulting from the 0xA4 word modulated with manchester encoding, reflected by TR #1. The RF input power entering the TR is $P_{in} = -55$ dBm and its output was directly injected into the RF receiver.

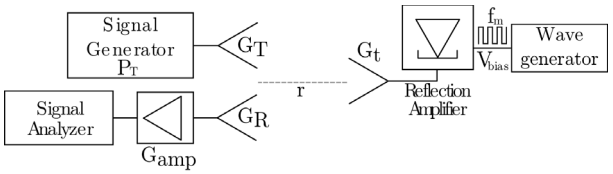

Fig. 20. Experimental setup to test the wireless capabilities of a tunneling tag. $P_T = -20$ dBm, $G_T = G_t = 6$ dBi, $G_R = 12$ dBi, $G_{amp} = 30$ dB, $r = 23$ m, $f_m = 250$ kHz.

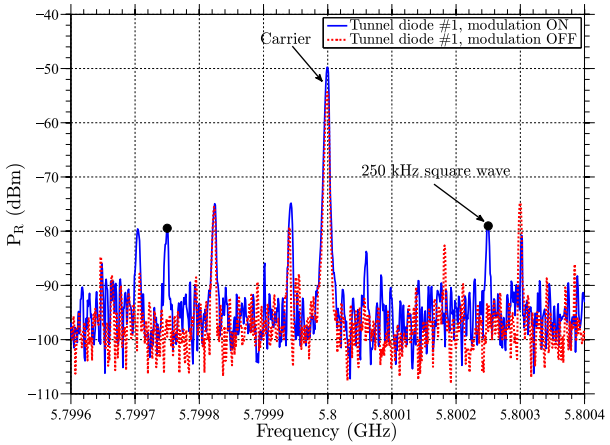

Fig. 21. Signal backscattered by the tunneling RFID tag and observed at the reader ($r = 23$ m). When the tag is biased with a 250 kHz square wave ($V_{pp} = 69$ mV), peaks at 250 kHz away from the carrier frequency are observed. Other frequencies from other surrounding signals are present when the modulation is turned both ON and OFF. Spectrum analyzer setup: resolution BW 3 kHz, video BW 100 kHz, sweeping time 97 ms on 1001 points.

at 10 Msps, resulting in a Nyquist frequency of 5 MHz in the time domain; the base-band I and Q data were then read and sampled by an analog to digital converter (ADC). The obtained results are illustrated in Fig. 19 and compared with an ideal waveform; a gain of a about 20 dB was observed in line with the data points from Fig. 15.

To test the wireless capabilities, the setup in Fig. 20 was used. A tunneling tag was assembled by connecting the TR#1 to a patch antenna with gain $G_t = 6$ dBi at 5.8 GHz. Differently from a typical RFID tag, the tunneling tag uses a

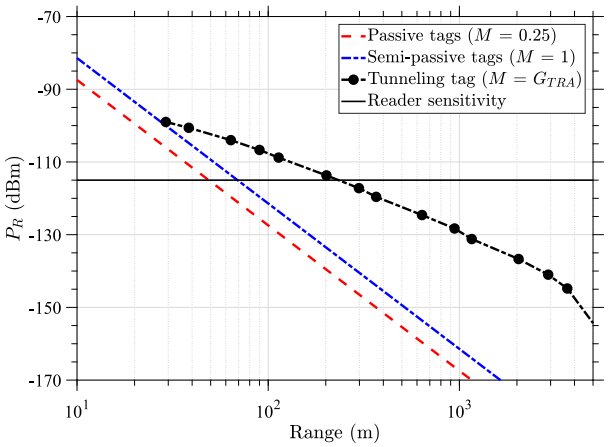

Fig. 22. Backscattering link budget estimation: $P_T = 30$ dBm, $G_T = G_R = G_t = 6$ dBi, $f_{in} = 5.8$ GHz. The return gains from Fig. 15 were used as the tunneling reflector gain G_{TR}. The 6 dB shift between the ideal passive and the ideal semi-passive tags is due to the different modulation factors M; the different slope of the tunneling tag link budget is due to the dependence of G_{TR} on the RF power level impinging on it. The tunneling tag prototype could achieve hundreds of meter ranges.

biasing source to modulate the backscattered signal by turning on and off the tunnel diode. The tag is biased with a square wave of 69 mV in amplitude and a modulating frequency, f_m, of 250 kHz. The reader was assembled to transmit the 5.8 GHz CW and to receive the backscatter signals; it consisted of a signal generator, a transmitting patch antenna with gain $G_T = 6$ dBi, and a receiving antenna, $G_R = 12$ dBi, connected to a signal analyzer through a 30 dB amplifier. The reader transmitted a 5.8 GHz CW of -14 dBm (EIRP) toward the tunneling tag located 23 meters away. The tag detected the attenuated impinging RF signal ($P_{in} = -83$ dBm) and backscattered it upon amplification. With no reflection gains, a received power of $P_R = -110$ dBm was expected; nevertheless, a backscattered signal of -78 dBm was detected at the receiving section of the reader when the modulating biasing voltage of the tunneling tag was turned on (Fig. 21). This results in a 32 dB gain added to the modulated backscattered signal by the tunneling reflector.

V. Conclusion

This work describes the design and testing of a Tunneling Reflector and anticipates how a Tunneling Tag based on tunnel diodes can backscatter, modulate and amplify an impinging RF signal in RFID applications. The tunneling effect exploited in the presented prototypes gave high return gains (up to 40 dB) with low bias power requirements (less than 45 μW) at 5.8 GHz ISM band for RF input power levels as low as -84 dBm and up to -40 dBm. Moreover, a tunneling RFID tag achieved a communication range of 23 meters when a 5.8 GHz continuous wave of -14 dBm (EIRP) was transmitted.

Using the experimental data in Fig. 15 of TR#1 as the tag modulation factor M, the achievable ranges of a 5.8 GHz tunneling tag were estimated through Eq. (1). The results are shown in Fig. 22 and compared with the achievable ranges of

ideal 5.8 GHz passive and semi-passive tags when transmitting a 36 dBm CW (EIRP): at high distances, the tunneling tag reaches a range of 200 m in an RFID link while keeping the bias power one order of magnitude lower than other reported reflection amplifiers. Since a 5.8 GHz RFID reader is not commercially available, a receiver sensitivity of -115 dBm was chosen as achievable reference. For the receiver, the overall bit detection sensitivity is a function of noise bandwidth and signal coding [37]. Manchester coding at 250 kHz requires a noise bandwidth of 500 kHz and no coding gain is added. Assuming an ideal receiver with a Noise Figure of 0 dB, the sensitivity of the receiver is $kTB = -115$ dBm (where k is the Boltzmann constant, T is the receiver temperature, 300 K, and B is the noise bandwidth, 500 kHz).

While passive tags have a maximum sensitivity of -22.1 dBm [38] that corresponds to a maximum *forward* link range of 6.6 m at 5.8 GHz, tunneling tags, by being sensitive to RF input signals as low as -85 dBm, can reach a theoretical *forward* link of 9 km.[2] Moreover, field test campaigns [1], [2] demonstrated that the *backscattering link* of a Tunneling Tag goes beyond (> 650 m) the values estimated and shown in Fig. 22.

Tunneling Tags can play a key role in enhancing RFID communication ranges without significantly affecting the low power budget of a typical RFID tag and be a valid alternative to currently available semi-passive RFID transponders. This work provides a starting point for research in enhanced RFID links through the use of tunnel diodes; the long range backscattering capabilities of a Tunneling Tag have been already demonstrated in [1] and AmatoTWC2018, and several other directions can be undertaken: a TR as modulating load for Van Atta arrays [39] or rat-race couplers [40] can retain the field-of-view of the single-antenna Tunneling Tag and further extend its range thanks to the array gain; moreover, controlling the phase and magnitude of the reflected RF signal of a TR, QAM modulation can be implemented [41]. A power efficiency study [33] of the TR can further improve the gain performances of the prototype; finally, by requiring extremely low bias power levels, an energy harvesting module [42] can expand the design presented in this work opening the doors for a new generation of long range, high bandwidth passive tags.

REFERENCES

[1] F. Amato, H. M. Torun, and G. D. Durgin, "Beyond the limits of classic backscattering communications: A quantum tunneling RFID tag," in *Proc. IEEE Int. Conf. RFID (RFID)*, May 2017, pp. 20–25.

[2] F. Amato, H. M. Torun, and G. D. Durgin, "RFID backscattering in long-range scenarios," *IEEE Trans. Wireless Commun.*, vol. 17, no. 4, pp. 2718–2725, Apr. 2018.

[3] S. Khaledian, F. Farzami, D. Erricolo, and B. Smida, "A full-duplex bidirectional amplifier with low DC power consumption using tunnel diodes," *IEEE Microw. Compon. Lett.*, vol. 27, no. 12, pp. 1125–1127, Dec. 2017.

[4] F. Farzami, S. Khaledian, B. Smida, and D. Erricolo, "Ultra-low power reflection amplifier using tunnel diode for RFID applications," in *Proc. IEEE Int. Symp. Antennas Propag. USNC/URSI Nat. Radio Sci. Meeting*, Jul. 2017, pp. 2511–2512.

[2]Link budget measured for a 36 dBm EIRP and a 6 dBi gain receiving tag antenna.

[5] F. Amato, C. W. Peterson, M. B. Akbar, and G. D. Durgin, "Long range and low powered RFID tags with tunnel diode," in *Proc. IEEE Int. Conf. RFID Technol. Appl. (RFID-TA)*, Sep. 2015, pp. 182–187.

[6] F. Amato, C. W. Peterson, B. P. Degnan, and G. D. Durgin, "A 45 μw bias power, 34 dB gain reflection amplifier exploiting the tunneling effect for RFID applications," in *Proc. IEEE Int. Conf. RFID (RFID)*, Apr. 2015, pp. 137–144.

[7] J. Kimionis *et al.*, "An enhanced-range RFID tag using an ambient energy powered reflection amplifier," in *Proc. IEEE MTT-S Int. Microw. Symp. (IMS)*, Jun. 2014, pp. 1–4.

[8] P. Chan and V. Fusco, "Full duplex reflection amplifier tag," *IET Microw. Antennas Propag.*, vol. 7, no. 6, pp. 415–420, Apr. 2013.

[9] A. Lazaro, A. Ramos, R. Villarino, and D. Girbau, "Time-domain UWB RFID tag based on reflection amplifier," *IEEE Antennas Wireless Propag. Lett.*, vol. 12, pp. 520–523, 2013.

[10] V. Vesterinen, J. Hassel, and H. Seppa, "Tunable impedance matching for Josephson junction reflection amplifier," *IEEE Trans. Appl. Supercond.*, vol. 23, no. 3, Jun. 2013, Art. no. 1500104.

[11] J.-F. Bousquet, S. Magierowski, and G. G. Messier, "A 4-GHz active scatterer in 130-nm CMOS for phase sweep amplify-and-forward," *IEEE Trans. Circuits Syst. I, Reg. Papers*, vol. 59, no. 3, pp. 529–540, Mar. 2012.

[12] P. Chan and V. Fusco, "Bi-static 5.8 GHz RFID range enhancement using retrodirective techniques," in *Proc. IEEE Eur. Microw. Conf. (EuMC)*, Oct. 2011, pp. 976–979.

[13] H. Cantu, V. Fusco, and S. Simms, "Microwave reflection amplifier for detection and tagging applications," *IET Microw. Antennas Propag.*, vol. 2, no. 2, pp. 115–119, Mar. 2008.

[14] H. I. Cantu and V. F. Fusco, "A 21 GHz reflection amplifier MMIC for retro-directive antenna and RFID applications," in *Proc. Inst. Eng. Tech. Seminar MM-Wave Products Tech.*, Nov. 2006, pp. 66–70.

[15] S.-J. Chung, S.-M. Chen, and Y.-C. Lee, "A novel bi-directional amplifier with applications in active Van Atta retrodirective arrays," *IEEE Trans. Microw. Theory Techn.*, vol. 51, no. 2, pp. 542–547, Feb. 2003.

[16] P. Gardner and D. K. Paul, "Aspects of the design of low noise, negative resistance, reflection mode transistor amplifiers," *IEEE Trans. Microw. Theory Techn.*, vol. 39, no. 11, pp. 1869–1875, Nov. 1991.

[17] S. Nicotra, "13 GHz FET negative resistance 0.5 W amplifier," in *Proc. IEEE Eur. Microw. Conf.*, Sep. 1979, pp. 303–307.

[18] G. C. Dalman, F. G. Zappert, and C. A. Lee, "Relaxing-avalanche-mode reflection amplifier," *Electron. Lett.*, vol. 8, no. 9, pp. 243–244, May 1972.

[19] D. M. Dobkin, *The RF in RFID*. Oxford, U.K.: Elsevier, 2013.

[20] J. D. Griffin and G. D. Durgin, "Complete link budgets for backscatter-radio and RFID systems," *IEEE Antennas Propag. Mag.*, vol. 51, no. 2, pp. 11–25, Apr. 2009.

[21] F. Amato and G. D. Durgin, "Signal-to-noise ratio measurements for IoT communications with quantum tunneling reflectors," in *Proc. IEEE World Forum IoT*, Dec. 2016, pp. 383–388.

[22] K. Chang, *Microwave Solid-State Circuits and Applications*. New York, NY, USA: Wiley, 1994.

[23] L. Drabeck, M. Schneider, and C. Tran, "Detector and modulator circuits for passive microwave links," U.S. Patent 5 598 169, Jan. 28, 1997. Accessed: Jun. 7, 2018. [Online]. Available: https://www.google.ch/patents/US5598169

[24] M. K. McPhun, "U.H.F. tunnel-diode amplifier," *Inst. Elect. Eng.*, vol. 114, no. 4, pp. 428–434, Apr. 1967.

[25] W. T. Read, "A proposed high-frequency, negative resistance diode," *Bell Syst. Tech. J.*, vol. 37, no. 2, pp. 401–446, Mar. 1958.

[26] S. Chung, S. Chen, and Y. Lee, "Microwave oscillations of current in III-V semiconductors," *Solid-State Commun.*, vol. 1, no. 4, pp. 89–91, Sep. 1963.

[27] B. K. Ridley and T. B. Watkins, "The possibility of negative resistance effects in semiconductors," *Proc. Phys. Soc.*, vol. 78, no. 2, p. 293, 1961.

[28] C. Hilsum, "Transferred electron amplifiers and oscillators," *Proc. IRE*, vol. 50, no. 2, pp. 185–189, Feb. 1962.

[29] L. Esaki, "New phenomenon in narrow germanium p-n junctions," *Phys. Rev.*, vol. 109, no. 2, pp. 603–604, Jan. 1958. Accessed: Jun. 7, 2018. [Online]. Available: http://link.aps.org/doi/10.1103/PhysRev.109.603

[30] L. Esaki, "Long journey into tunneling," *Proc. IEEE*, vol. 62, no. 6, pp. 825–831, Jun. 1974.

[31] A. Seabaugh *et al.*, "Transistors and tunnel diodes for analog/mixed-signal circuits and embedded memory," in *Int. Tech. Dig. Electron Devices Meeting*, Dec. 1998, pp. 429–432.

[32] S. Hemour and K. Wu, "Radio-frequency rectifier for electromagnetic energy harvesting: Development path and future outlook," *Proc. IEEE*, vol. 102, no. 11, pp. 1667–1691, Nov. 2014.

[33] C. H. P. Lorenz *et al.*, "Breaking the efficiency barrier for ambient microwave power harvesting with heterojunction backward tunnel diodes," *IEEE Trans. Microw. Theory Techn.*, vol. 63, no. 12, pp. 4544–4555, Dec. 2015.
[34] RFMW. (2011). *Planar Back (Tunnel) Diodes MBD Series*. Accessed: Jun. 7, 2018. [Online]. Available: https://www.rfmw.com/ProductDetail/MBD5057E28-metelics/472882/
[35] OshPark. (2014). *4 Layer Prototype Service*. Accessed: Jun. 7, 2018. [Online]. Available: http://docs.oshpark.com/services/four-layer/
[36] Isola. (2014). *FR408 High Performance Laminate and Prepreg*. Accessed: Jun. 7, 2018. [Online]. Available: http://docs.oshpark.com/resources/FR408-High-Performance-Laminate-and-Prepreg-Data-Sheet.pdf
[37] G. D. Durgin *et al.*, "Modulation and sensitivity limits for backscatter receivers," in *Proc. IEEE RFID Int. Conf.*, Apr. 2013, pp. 124–130.
[38] Impinj. (2015). *Monza R6 RFID Tag Chip*. Accessed: Jun. 7, 2018. [Online]. Available: http://www.impinj.com/products/tag-chips/monza-r6/
[39] F. Farzami, S. Khaledian, B. Smida, and D. Erricolo, "Reconfigurable dual-band bidirectional reflection amplifier with applications in Van Atta array," *IEEE Trans. Microw. Theory Techn.*, vol. 65, no. 11, pp. 4198–4207, Nov. 2017.
[40] M. Alhassoun, M. A. Varner, and G. D. Durgin, "Design and evaluation of a multi-modulation retrodirective RFID tag," in *Proc. IEEE Int. Conf. RFID (RFID)*, 2018, pp. 1–8.
[41] S. J. Thomas, E. Wheeler, J. Teizer, and M. S. Reynolds, "Quadrature amplitude modulated backscatter in passive and semipassive UHF RFID systems," *IEEE Trans. Microw. Theory Techn.*, vol. 60, no. 4, pp. 1175–1182, Apr. 2012.
[42] C. H. P. Lorenz, S. Hemour, and K. Wu, "Physical mechanism and theoretical foundation of ambient RF power harvesting using zero-bias diodes," *IEEE Trans. Microw. Theory Techn.*, vol. 64, no. 7, pp. 2146–2158, Jul. 2016.

Francesco Amato received the B.S. and M.S. degrees in telecommunication engineering from the University of Roma Tor Vergata in 2006 and 2009, respectively, and the Ph.D. degree in electrical and computer engineering from the Georgia Institute of Technology, Atlanta, GA, USA, in 2017. He is currently a Post-Doctoral Researcher with the Sant'Anna School of Advanced Studies, Pisa. From 2009 to 2011, he was with SES, Luxembourg, as a Ground System Engineer. In 2012, he joined the Propagation Group with the Georgia Institute of Technology as a Fulbright Research Scholar. He was a Research Intern with Intel Labs, Santa Clara, CA, USA. His current research interests include microwave photonics and backscatter radio communications. He was a recipient of the Master Thesis Prize *Sebastiano e Rita Raeli* in 2009, the Fulbright Scholarship in 2012, the GoSTEM Fellowships in 2013 and 2014, the Best Student Paper Award of the IEEE International Conference on RFID-Technologies and Applications in 2015, Tokyo, Japan, and the William Brown Fellowship in 2015. He is the Organizing Committee Member for the 2017 and 2018 IEEE International Conference on RFID.

Christopher W. Peterson received the B.S. degree in electrical engineering from the Georgia Institute of Technology in 2015 and the M.S. degree in electrical engineering from the University of Illinois at Urbana–Champaign in 2018, where he is currently pursuing the Ph.D. degree. His current research interests include nonreciprocity, active and time-varying circuits, and topological insulators.

Brian P. Degnan received the degrees in mechanical and computer engineering from the Rose–Hulman Institute of Technology in 2000 and 2003, respectively, and the Ph.D. degree in electrical and computer engineering from the Georgia Institute of Technology in 2013. His research interest includes low-power electronics, such as subthreshold digital implementations, mixed-signal, and subthreshold systems and techniques.

Gregory D. Durgin received the B.S.E.E., M.S.E.E., and Ph.D. degrees from Virginia Polytechnic Institute and State University in 1996, 1998, and 2000, respectively. He joined the faculty of the School of Electrical and Computer Engineering, Georgia Tech, in 2003, where he serves as a Professor. He was a Visiting Researcher with Morinaga Laboratory, Osaka University for one year. He has authored the book entitled *Space-Time Wireless Channels*, the first textbook in the field of space-time channel modeling. He founded the Propagation Group with Georgia Tech, a research group that studies radiolocation, channel sounding, backscatter radio, RFID, and applied electromagnetics. He was a recipient of the Japanese Society for the Promotion of Science Post-Doctoral Fellowship in 2001, the best paper awards for articles co-authored in the IEEE TRANSACTIONS ON COMMUNICATIONS (Stephen O. Rice Prize) in 1998, the *IEEE Microwave Magazine* in 2014, and IEEE RFID Conference in 2016, the NSF CAREER Award as well as numerous teaching awards, including the Class of 1940 Howard Ector Outstanding Classroom Teacher Award at Georgia Tech in 2007. He has served as an Editor for the *IEEE RFID Virtual Journal*, the IEEE TRANSACTIONS ON WIRELESS COMMUNICATIONS, and IEEE JOURNAL OF RADIO FREQUENCY IDENTIFICATION. He also serves on the Advisory Committee on the IEEE Council for RFID (ComSoc Liaison). He is a frequent consultant to industry, having advised many multinational corporations on wireless technology.